Research Article

Progressive Damage Process and Failure Characteristics of Coal under Uniaxial Compression with Different Loading Rates

Chuanqi Zhu [iD],[1] **Shaobo Li** [iD],[1] **Yong Luo** [iD],[1,2] **and Biao Guo** [iD][3]

[1]*State Key Laboratory of Mining Response and Disaster Prevention and Control in Deep Coal Mines, Anhui University of Science and Technology, Huainan 232001, China*
[2]*School of Resources Environment and Safety Engineering, University of South China, Hengyang 421001, China*
[3]*Qidong Coal Mine of Hengyuan Coal Power Co., Ltd., Suzhou 234000, China*

Correspondence should be addressed to Shaobo Li; 2020080@aust.edu.cn

To study the effect of loading rate on the progressive damage and failure characteristics of coal, an ultrasonic detector and a camera were used to measure the P-wave velocity and record the failure process of cuboid coal samples in uniaxial compression tests with five loading rates. The mechanical properties, damage process, and failure characteristics of the samples were analysed, and the mechanism of the advancing velocity of the working face in coal failure was discussed. The results show that, as the loading rate increases, the peak strength of the sample generally shows an increasing trend, but the elastic modulus changes irregularly. The sample is more prone to local failure before the peak strength. An increase in the loading rate rapidly promotes damage in the sample and accelerates the transition from internal damage to macroscopic failure, with no obvious effect on the ratio of damage threshold to corresponding peak strength. At low loading rates, the samples mainly experienced static failure; the failure form was spalling, and the failure range was wide. At high loading rates, the samples were prone to dynamic failure in the local area, manifested as the ejection of slabs and debris. A greater loading rate produced smaller and thinner slabs and a greater ejection velocity. Properly increasing the advancing velocity of the working face is conducive to reducing spalling to prevent large-area roof fall, but it may increase the possibility of coal burst in local areas. The results of this study provide a reference for roof control and coal burst disaster prevention on the working face in deep coal mining.

1. Introduction

As economic development increases the demand for energy and shallow coal resources are gradually depleted, coal mining is forced into the deep underground [1–6]. In deep mining, the geological and geostress environment of the coal becomes more complicated and varied. Under the influence of high geostress and strong mining, the coal in front of the working face is prone to spalling [7, 8], inducing rock and coal burst disasters in severe cases [9–14]. With the increasing scale of coal mining and degree of mechanization, the advancing velocity of the working face increases, increasing the likelihood of dynamic disasters, especially in hard coal, threatening safe and efficient mining of coal resources [15–18].

The advancing velocity of the working face has an impact on the transfer and concentration process of the mining stress in the coal, resulting in different loading rates on the coal caused by the abutment pressure. The change in loading rate affects the deformation, strength, and failure of the coal, and increased loading rates increase the possibility of coal failure [19]. To investigate the impact of loading rate on the mechanical properties and failure characteristics of coal, researchers have conducted many compression tests on coal with different loading rates. Huang and Liu [20] conducted uniaxial compression tests on coal-rock combinations at different loading rates and reported that high loading rates increased the ability of coal rock to convert external energy into elastic strain energy, making it more prone to unsteady failure. Okubo et al. [21] conducted uniaxial compression

and uniaxial tensile tests on coal and found that the influence of the loading rate on the uniaxial compression and tensile peak strength of coal was relatively low. Huang et al. [22] performed cyclic loading-unloading tests on coal at different loading rates and studied the effect of loading rate on the mechanical and creep characteristics of coal. Li et al. [23] conducted uniaxial compression tests on coal with different loading rates and studied the effect of loading rate on the mechanical and acoustic emission characteristics of coal. They noted that the loading rate has a significant influence on the peak stress, but a small influence on the elastic modulus, and that the cumulative number of acoustic emissions was negatively correlated with the loading rate. Ai et al. [24] performed triaxial loading-unloading tests on coal at different loading rates and studied the effect of loading rate on coal acoustic emission evolution and energy release characteristics. It was found that a greater loading rate produced earlier AE activity and main failure and that the coal failure changed from brittleness to ductility at the critical loading rate. Chen et al. [25] conducted a uniaxial compression test on coal-rock combinations and reported that as the loading rate increased, the peak strength increased slightly and the stress threshold increased linearly. Wang et al. [26] conducted uniaxial compression tests on coal-rock combinations at different loading rates and found that as the loading rate increased, the strength showed an increasing trend, and the failures of the samples were progressive shear failure, splitting failure, and structural failure. Li et al. [27] studied the effect of loading rate on mechanical properties of coal and reported that as the loading rate increased, the ultimate stress and strain of the sample first decreased and then increased. Xiao et al. [28] performed a uniaxial compression test on coal and found that as the loading rate increased, the peak stress and total absorbed energy of the samples increased continuously, with debris splashing occurring at some loading rates. These studies can provide guidance for understanding the influence of loading rate on coal mechanical properties and failure characteristics. It is difficult to meet the increasingly complex mining requirements; few studies have studied the impact of loading rate on the coal damage process by measuring longitudinal wave velocity in real time during experimental loading.

In this study, uniaxial compression tests were performed on cuboid coal samples at five loading rates. The P-wave velocity of the samples during the loading process was measured with an ultrasonic detector in real time, and the failure process of the samples was recorded using a high-definition camera. The mechanical properties, damage and failure process, and failure characteristics of samples with different loading rates were analysed in detail, and the mechanism of the advancing velocity of the working face in coal failure was studied. The results can provide guidance for the prevention of coal burst in deep coal mining.

2. Experimental Method

2.1. Sample Preparation.
To facilitate measurement of the P-wave velocity during the sample loading process, the collected coal block was processed into cuboid samples (50 mm × 50 mm × 100 mm, Figure 1). The upper and lower end surfaces of the sample were polished to control the surface flatness within ±0.02 mm. Samples without obvious structural surfaces were selected for testing.

2.2. Experimental Apparatus.
An MTS816 rock mechanics testing system was used to perform uniaxial compression loading tests on cuboid samples at different loading rates. To ensure the reliability of the test results, two tests were conducted at each loading rate. During the test, a ZBL-U510 nonmetal ultrasonic detector was used to measure the P-wave velocity of the samples in real time; the failure process of the samples was recorded using a high-definition camera. The installation and layout of the experiment are shown in Figure 2.

2.3. Experimental Scheme.
To investigate the effect of loading rate on the progressive damage process and failure characteristics of coal, five loading rates (0.002 mm/min, 0.004 mm/min, 0.006 mm/min, 0.008 mm/min, and 0.01 mm/min) were set for uniaxial compression tests on coal samples. During the test, samples were continuously loaded until overall failure occurred. When the axial deformation reached 0.1 mm, the P-wave velocity of the samples was measured once with an ultrasonic detector to obtain the change in the P-wave velocity during the entire loading process at different loading rates. A high-definition camera was used to record the failure process of the samples at different loading rates.

3. Test Results and Analysis

3.1. Mechanical Properties of Samples.
After testing, stress-strain curves were obtained for different loading rates, as shown in Figure 3 (only one test stress-strain curve shown for each loading rate is given). The stress-strain curves exhibit significant differences with different loading rates, but the change trends of the curves are generally consistent. All of the stress-strain curves show a long compaction stage, which indicates that the coal contains a large number of original microcracks and cavities. In addition, the stress-strain curves indicate different degrees of stress drop before reaching the peak strength. This phenomenon is more obvious at low loading rate, indicating that local failure in the samples occurs before the stress reaches the peak strength. A lower loading rate produces a larger failure range, and an obvious stress drop is more likely to occur (at high loading rates, the local failure range of the samples is smaller).

From the stress-strain curves, the peak strength and elastic modulus of the samples were obtained at different loading rates, as presented in Table 1. Figure 4 shows the variation in peak strength and elastic modulus of the samples as the loading rate increases. The peak strength of the sample is relatively discrete at the same loading rate. At a loading rate of 0.01 mm/min, the difference between the peak strengths of the two samples was nearly 13 MPa. This may be the result of a structural weak surface inside samples with a
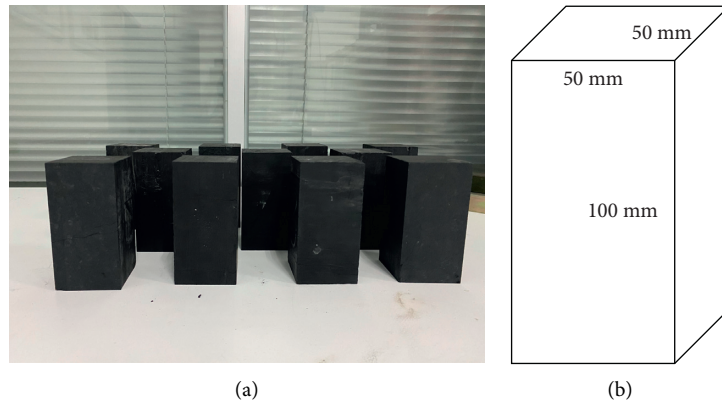
FIGURE 1: Experimental samples: (a) photo of samples and (b) sample dimensions.

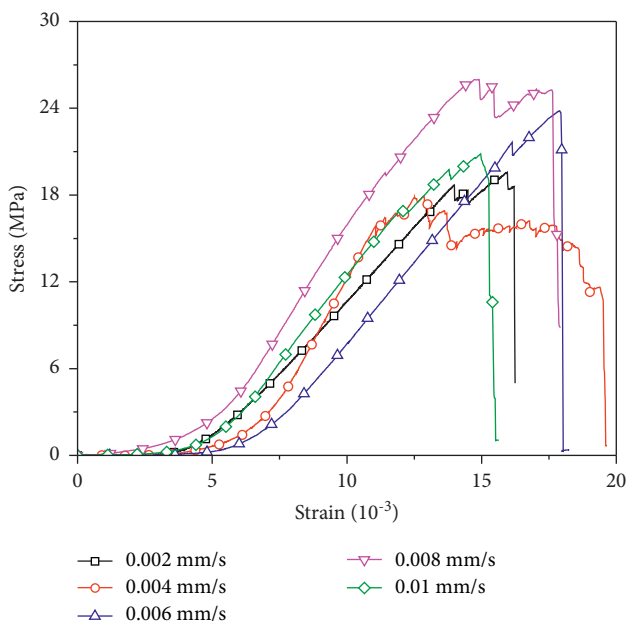FIGURE 2: Test equipment and its installation and layout.

FIGURE 3: Stress-strain curves of samples with different loading rates.

low peak strength; the initial P-wave velocity is significantly lower than that of high peak strength samples. The average peak strength shows an increasing trend as the loading rate increases, which is consistent with previous research results [28, 29]. The elastic modulus of the samples exhibits irregularities with an increase in loading rate, which is consistent with the results obtained by Wang et al. [18] and Li et al. [27]. Compared with other types of rocks, coal generally exhibits poor homogeneity and contains more structural weak surfaces [30], resulting in significant differences in coal deformation parameters.

3.2. Damage Process of Samples. The essence of the macro failure of coal is the result of crack propagation and coalescence caused by internal damage accumulation under the action of external force. Generally, the P-wave velocity better characterizes the internal damage of coal and continues to decrease with accumulation of internal damage. The P-wave velocity measured in the experiment was used to analyse the damage process of the samples at different loading rates. Figure 5 shows the relationship between the stress-strain curve and the P-wave velocity of the samples at different

TABLE 1: Physical and mechanical parameters of samples at different loading rates.

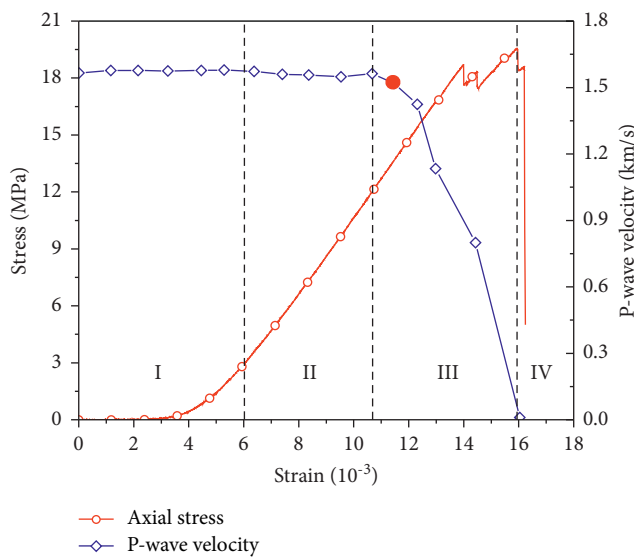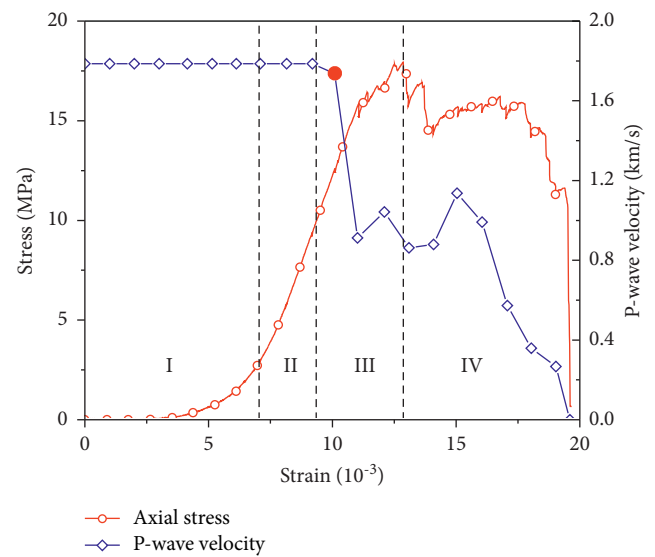| Loading rate (mm/min)	P-wave velocity (km/s)	Peak strength (MPa)	Average peak strength (MPa)	Elastic modulus (GPa)	Average elastic modulus (GPa)
0.002	1.57	19.57	21.88	2.03	2.11
	1.21	24.19		2.19	
0.004	1.79	17.93	21.94	3.47	2.83
	1.25	25.94		2.20	
0.006	1.44	23.82	22.34	2.25	2.16
	1.23	20.85		2.07	
0.008	1.31	25.99	24.23	2.92	2.53
	1.32	22.46		2.13	
0.010	0.99	20.84	27.18	2.42	2.08
	1.31	33.52		1.74	
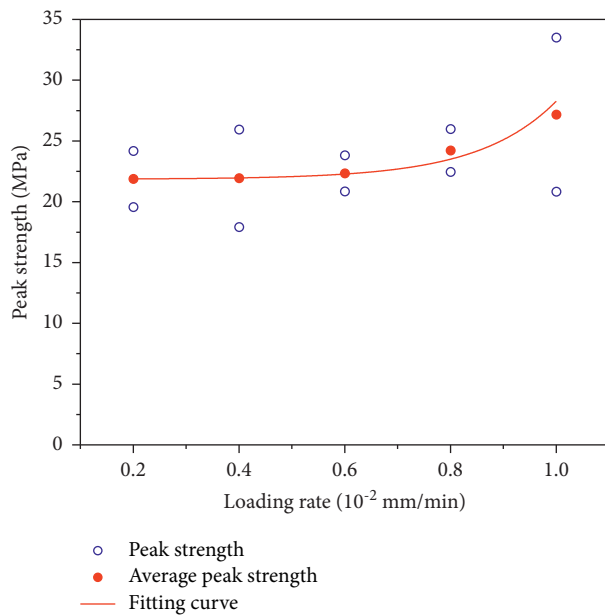
(a)
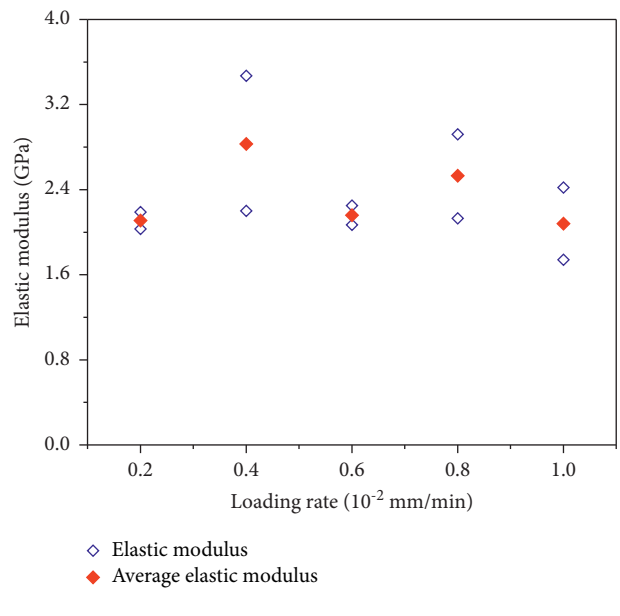
(b)

FIGURE 4: (a) Peak strength and (b) elastic modulus of samples at different loading rates.
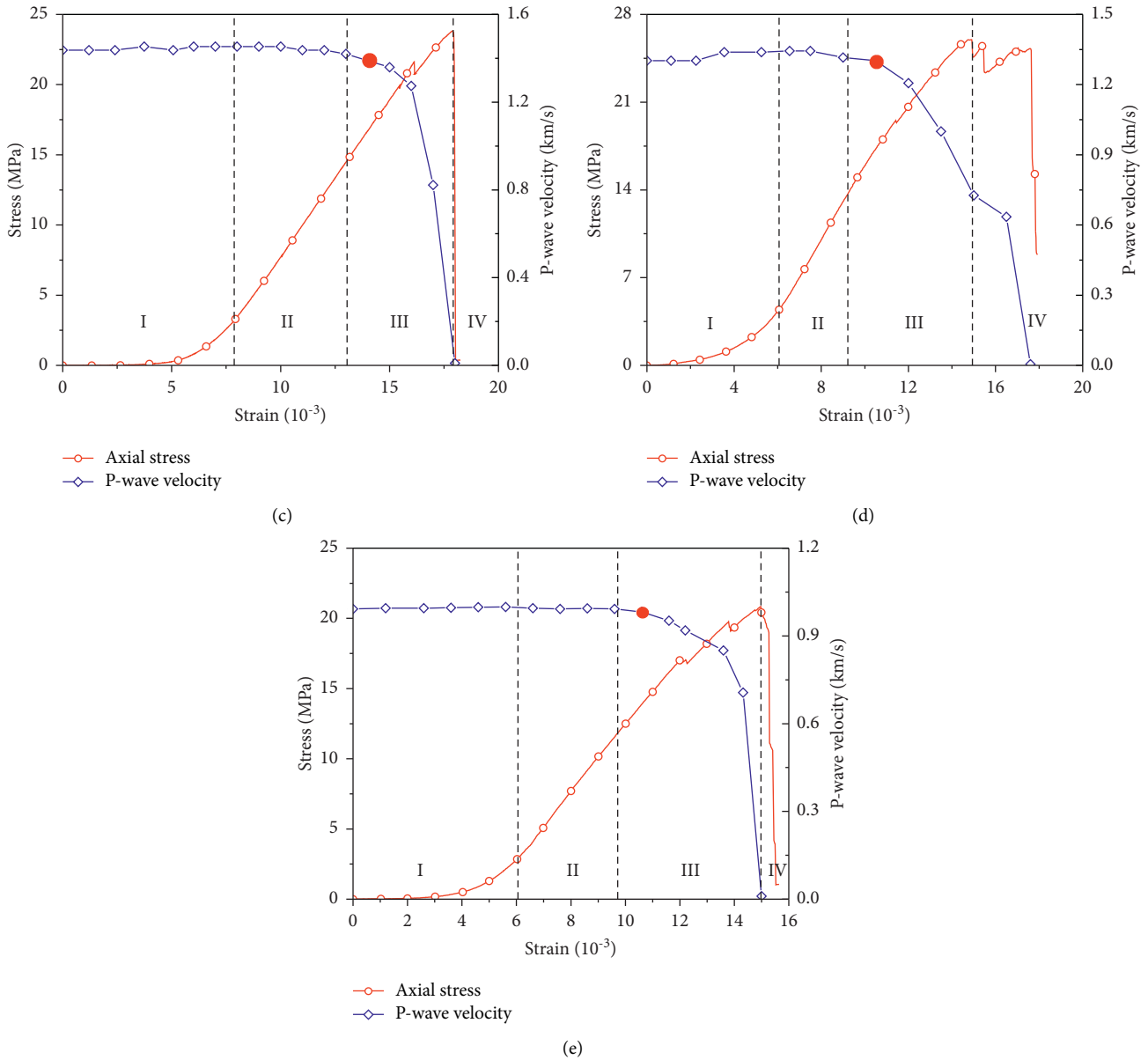

(a)

(b)

FIGURE 5: Continued.

(c)

(d)

(e)

FIGURE 5: Relationship between P-wave velocity and stress-strain of samples at different loading rates: (I) compaction stage, (II) elastic deformation stage, (III) yield stage, and (IV) postpeak stage. (a) 0.002 mm/min; (b) 0.004 mm/min; (c) 0.006 mm/min; (d) 0.008 mm/min; (e) 0.01 mm/min.

loading rates. Generally, the P-wave velocity does not change significantly during the compaction stage (I) and the elastic deformation stage (II) of the stress-strain curve, which indicates that the samples are not damaged in these stages. When the stress-strain curves enter the yield stage (III), the P-wave velocity of the samples first decreases slightly and then decreases rapidly before the peak strength. After the sample yields, a small amount of damage is slowly generated in the samples before damage occurs quickly; a large amount of damage is accumulated in the samples before reaching the peak strength. However, the P-wave velocity change process exhibits certain differences between samples. At low loading rates, the decreasing section of the P-wave velocity curves is

relatively inclined; at high loading rates, the decreasing section of the P-wave velocity curve is steeper. Once damage occurs inside the sample, damage occurs rapidly in a short time with a high loading rate. A red solid point is marked on the wave velocity curves in Figure 5 (indicating the turning point when the P-wave velocity begins to decrease significantly). From the P-wave velocity curve and the stress-strain curve, the axial stress corresponding to the red solid point (σ_a) can be obtained. Figure 6 shows the relationship between the ratio of σ_a to the peak strength (σ_p) of the sample and the loading rate. It is observed that σ_a/σ_p for the samples fluctuates between 0.6 and 0.7 and is not significantly affected by the loading rate. The effect of loading rate on the

damage of coal can be summarized as follows: when damage starts to occur in coal, the increasing loading rate accelerates the generation of damage, but has no significant effect on the ratio of damage threshold stress to the peak strength of the coal.

3.3. Failure Process and Characteristics of Samples. From the recorded videos during the test and the stress-strain curves (Figure 5), the failure process of each sample and the corresponding loading stress conditions at different loading rates can be obtained, as shown in Figure 7. For the sample with a loading rate of 0.002 mm/min, a splitting crack parallel to the left side was first generated in the lower-left corner when the axial stress reached 18.71 MPa, before the axial stress decreased to 17.62 MPa. A splitting crack parallel to the left side was subsequently generated in the upper-left corner when the axial stress increased to 18.32 MPa, before the axial stress decreased by 0.73 MPa. As the axial stress increased to the peak stress (19.57 MPa), the upper and lower splitting cracks on the left side coalesced, causing large pieces of coal to peel off and the acoustic probes to fall off when the axial stress decreased to 18.39 MPa. Splitting cracks approximately parallel to the left side appeared on the inner side of the spalling area; no obvious failure occurred in other areas (Figures 5(a) and 7(a)). For the sample with a loading rate of 0.004 mm/min, before reaching the peak stress, the axial stress fluctuated due to unstable propagation of the internal cracks. When the stress reached 17.39 MPa (peak stress), a crack appeared in the upper-right corner of the sample. After entering the postpeak stage, the axial stress continued to fluctuate, generally showing a downward trend. The crack in the upper-right corner gradually propagated to the lower-left corner and formed an inclined shear crack that penetrated the upper and lower end faces when the axial stress decreased to 11.04 MPa. Splitting cracks were generated at the bottom of the left and right sides; they continued to propagate upward, forming long cracks that penetrated the upper and lower end faces on the left side at an axial stress of 10.62 MPa, causing the acoustic probe to fall off (Figures 5(b) and 7(b)). For the sample with a loading rate of 0.006 mm/min, when the axial stress was loaded to 21.62 MPa, cracks were generated in the middle of the left side; ejection of slabs and debris occurred in the lower-right corner. When the peak stress was reached (23.82 MPa), ejection of slabs and debris occurred in the upper-left corner. The axial stress decreased to 21.12 MPa; the sample suddenly suffered severe failure, resulting in some splitting cracks and ejection of slabs and debris, causing the acoustic probe to fall off (Figures 5(c) and 7(c)). For the sample with a loading rate of 0.008 mm/min, there was no obvious failure before reaching the peak stress. When the stress reached the peak strength (25.99 MPa), splitting occurred in the lower-left corner. The crack continued to propagate upward, forming a long approximately V-shaped crack at an axial stress of 25.27 MPa. A small amount of debris and a large slab were ejected on the upper-right side at an axial stress of 25.23 MPa. With further loading, when the axial stress decreased to 15.21 MPa, slabs and debris were ejected at the upper-right corner, causing the acoustic probe to fall off (Figures 5(d) and 7(d)). For the sample with a loading rate of 0.01 mm/min, when the axial stress reached 19.24 MPa, failure occurred in the middle of the left side, causing the left probe to slide downward. As the stress increased to the peak stress (20.84 MPa), a large amount of powder was ejected on the upper-right side, followed by ejection of debris and slabs at the axial stress of 19.86 MPa, causing the right side probe to fall off. Subsequently, the axial stress dropped sharply to 11.1 MPa, a large amount of debris and slabs ejected on the upper left side (see Figures 5(e) and 7(e)). In addition, at all five loading rates, when the samples experienced macroscopic crack propagation or failure, a crisp tearing sound was heard; the sound became louder with increased loading rates.

From the analysis, at loading rates of 0.002 mm/min and 0.004 mm/min, the samples exhibited static failure, manifested mainly as spalling of slabs or static splitting. At loading rates of 0.006 mm/min, 0.008 mm/min, and 0.01 mm/min, the samples experienced dynamic failure, manifested mainly in the ejection of slabs and debris. To analyse the impact of the loading rate on the dynamic failure of the sample, the ejection failure process of the samples at loading rates of 0.006 mm/min, 0.008 mm/min, and 0.01 mm/min is presented in Figure 8. For the sample with a loading rate of 0.006 mm/min, the ejection of slabs and debris occurred suddenly at 08 : 15 : 720 (min:s:ms); the broken coal reached the left baffle in approximately 80 ms. The geometry of the ejected coal was mainly thick slabs and debris, and the ejection direction was mainly horizontal and toward the lower-left. The sample was severely damaged (Figure 8(a)). For the sample with a loading rate of 0.008 mm/min, failure occurred suddenly at 06 : 51 : 120 (min:s:ms); the ejected slabs and debris reached the right baffle in approximately 40 ms. The geometry of the ejected coal was primarily thin slabs and debris. The ejection direction was horizontal and toward the lower right and upper right. The sample failure was relatively severe (Figure 8(b)). For the sample with a loading rate of 0.01 mm/min, several layers of splitting cracks formed suddenly on the upper-right side at 07 : 27 : 120 (min:s:ms), accompanied by a spray of misty coal powder and ejection of thin slabs and debris; the broken coal reached the right baffle within 40 ms. The ejection direction was horizontal and toward the lower right and the upper right; the failure of the sample was relatively light (Figure 8(c)). It can be concluded that with an increased loading rate, the failure of the sample is more violent, the kinetic energy of the ejected coal is greater, the failure area is smaller (the sample is more prone to ejection failure in a local area), and the thickness of the slabs is smaller.

Thus, the loading rate has a significant impact on the failure of coal. At low loading rates, splitting is likely to occur near the free surface of the sample; the failure form is spalling (static failure), and the failure range runs through the entire height of the sample. As the loading rate increases, the failure form gradually changes from large-scale spalling to local ejection (the failure changes from static failure to dynamic failure). A greater loading rate produces a more violent ejection failure of the sample.
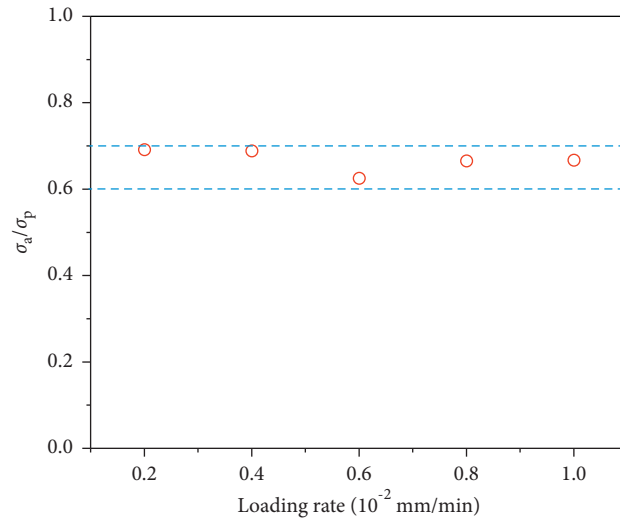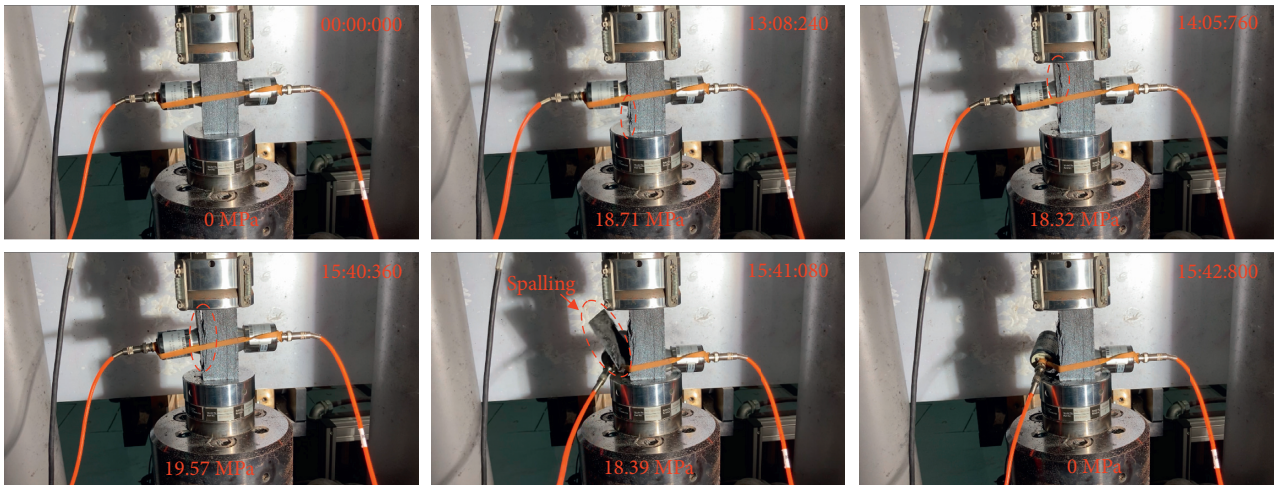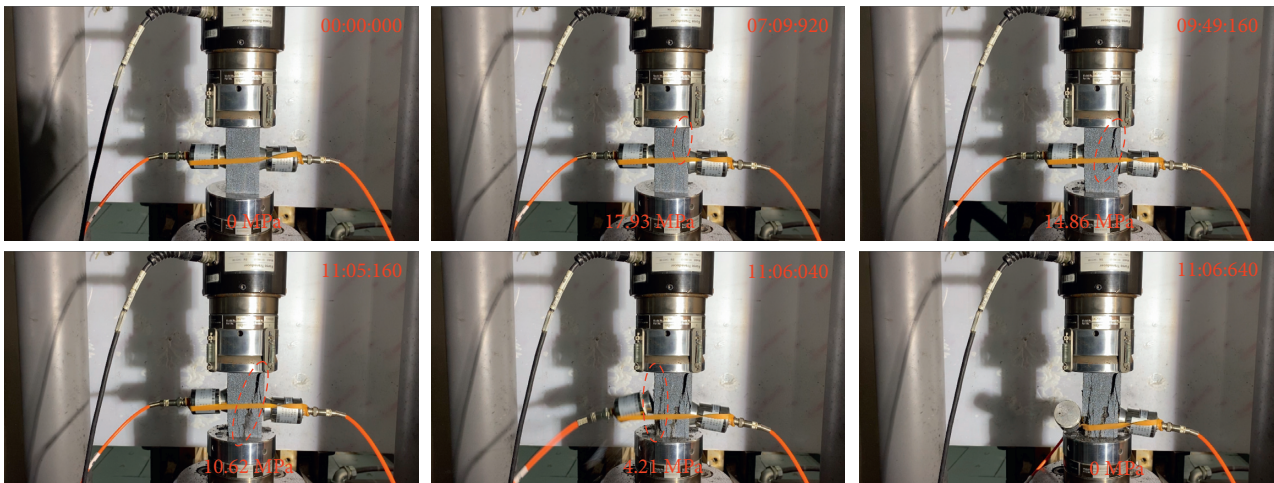
FIGURE 6: Influence of loading rate on σ_a/σ_p.
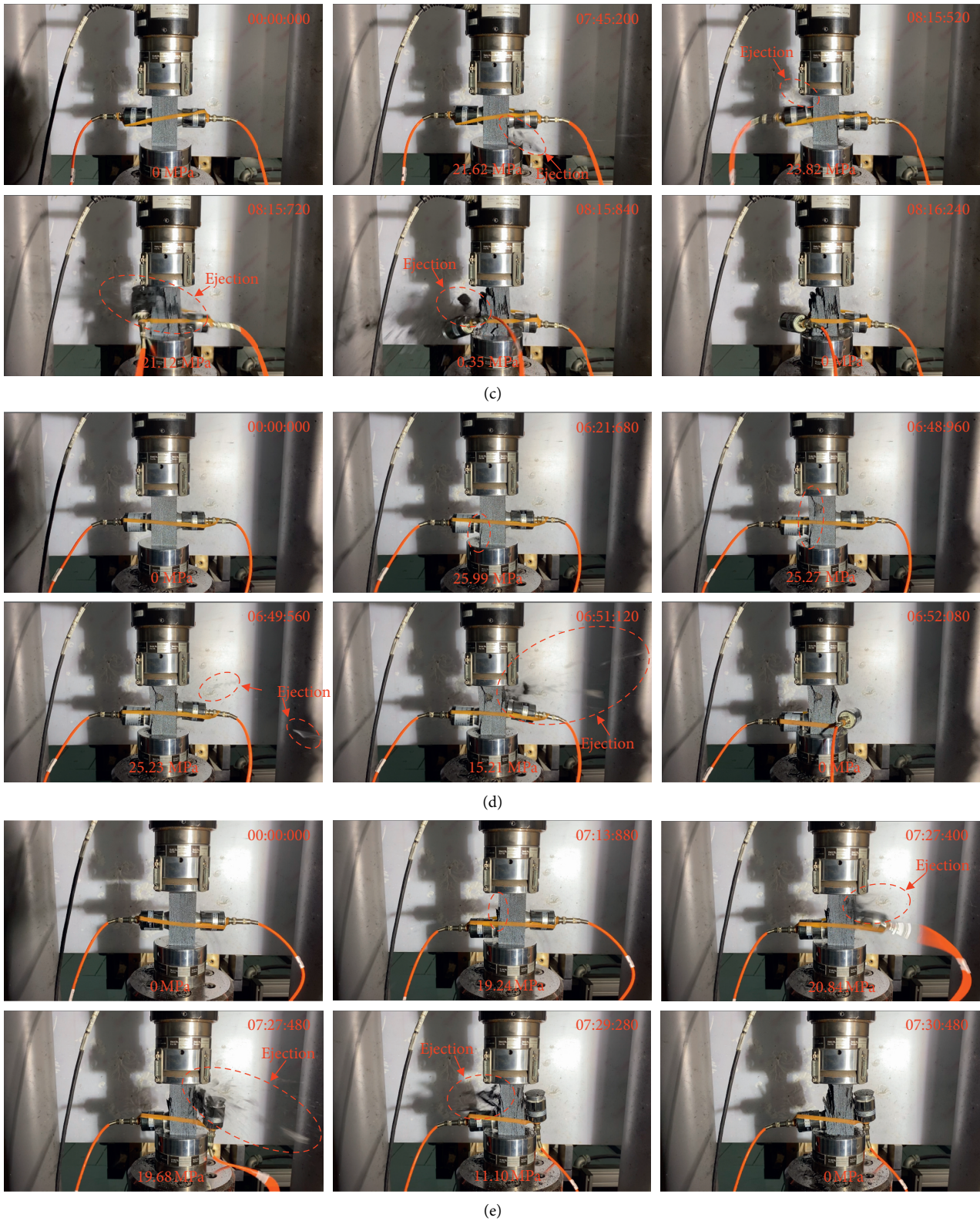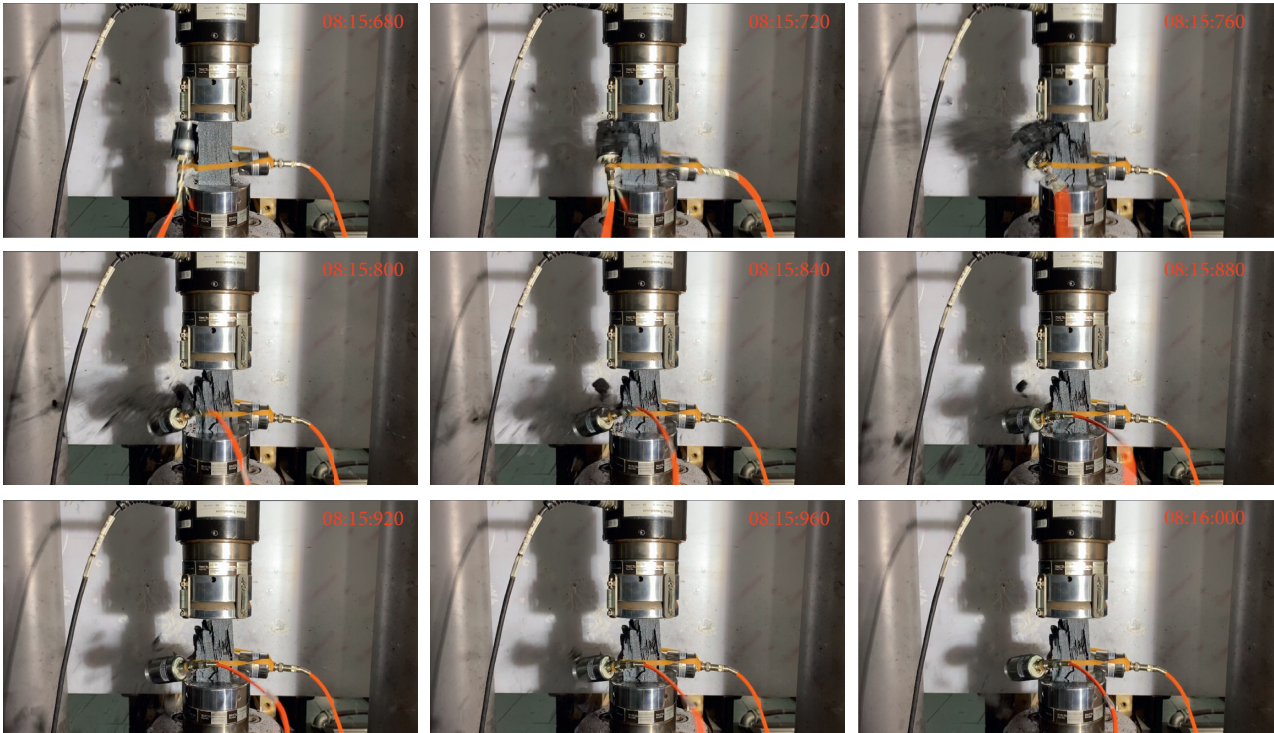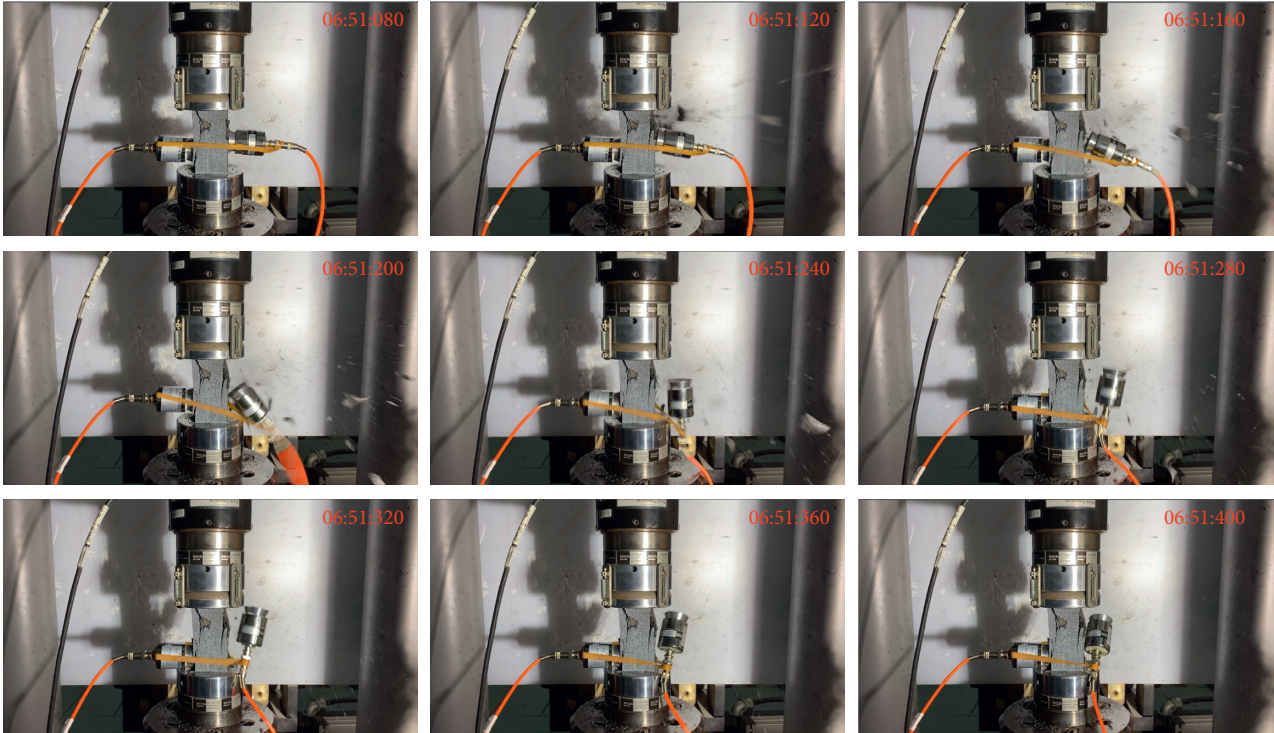

(a)

(b)

FIGURE 7: Continued.

Figure 7: Failure process of samples at different loading rates (the indicated stress is the axial stress at the corresponding loading moment): (a) 0.002 mm/min; (b) 0.004 mm/min; (c) 0.006 mm/min; (d) 0.008 mm/min; (e) 0.01 mm/min.
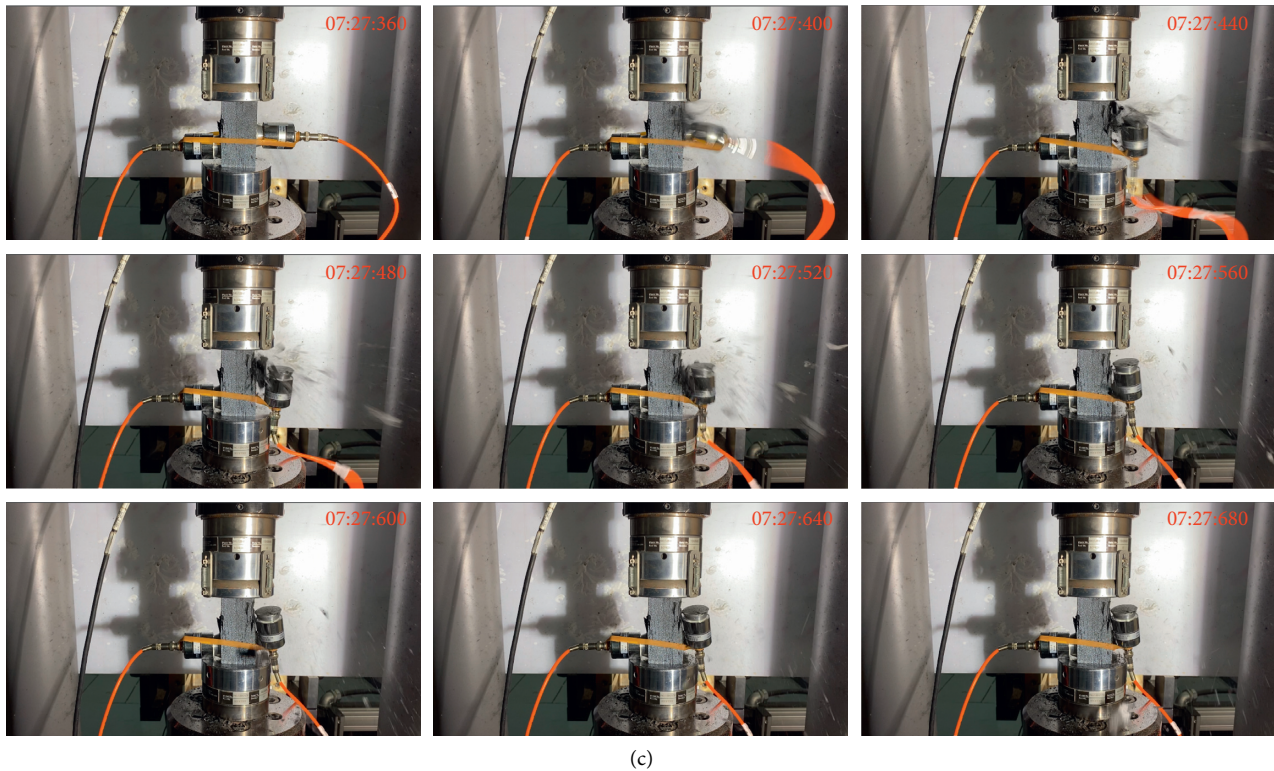
(a)

(b)

FIGURE 8: Continued.

(c)

FIGURE 8: Ejection process of samples at different loading rates: (a) 0.006 mm/min; (b) 0.008 mm/min; (c) 0.01 mm/min.

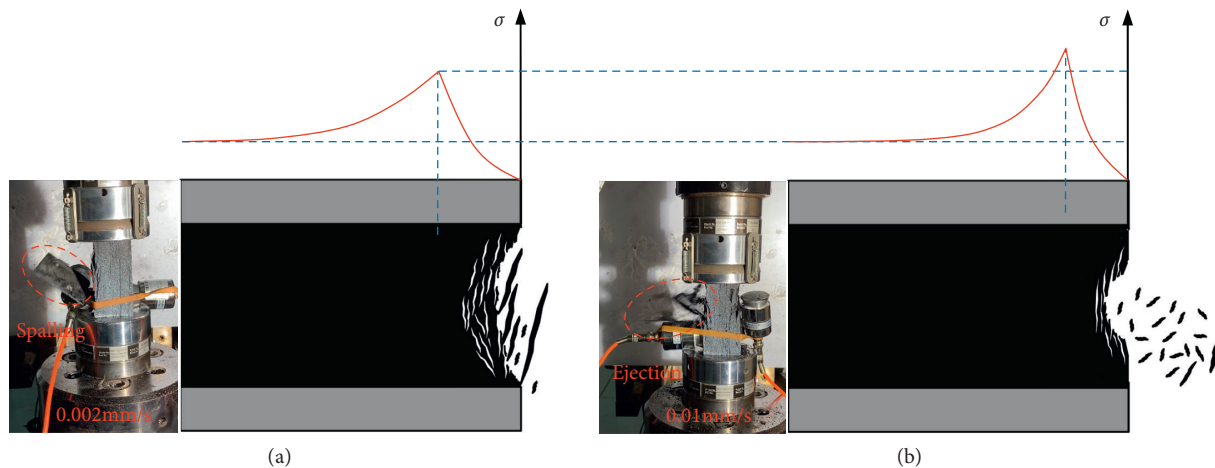(a)   (b)

FIGURE 9: Diagram of influence of advancing velocity of working face on coal wall failure: (a) low advancing velocity and (b) high advance velocity.

4. Discussion

Coal is a heterogeneous and anisotropic material with certain creep properties [31]. Under high stress, its deformation and failure are time dependent; thus, the mechanical properties and failure behaviour of coal exhibit a loading rate effect. For deep low gas coal mines (i.e., without considering the influence of gas on coal failure), the advancing velocity of the working face affects the transfer and concentration of mining stress and produces different loading rates on the

coal, which affects the stress redistribution and coal failure on the working face.

It is generally believed that a greater advancing velocity of the working face results in a greater loading rate on coal caused by mining stress [32, 33]. With a low advancing velocity of the working face, the mining stress exerts a low loading rate on the coal, and its internal cracks and plastic deformation can be well developed. The mining stress can be transferred to the deep coal; the strength of the coal is relatively low, resulting in relatively little elastic strain energy

stored in the coal. In this case, the failure zone in front of the working face is wider; the peak abutment pressure is relatively low, and the distance from the working face is relatively large; the failure of the coal at the working face is spalling, as shown in Figure 9(a). With a high advancing velocity of the working face, a high loading rate is applied to the coal; the bearing capacity (strength) of the coal increases, and its internal cracks and plastic deformation are not well developed; the mining stress is concentrated in a small area near the working face. In this case, the width of the failure zone is formed in the working face, and the peak bearing pressure is large and closer to the working face. The insufficient development of plastic deformation and cracks reduces the dissipated energy, and the increase in strength causes the coal to store more elastic strain energy, which can induce coal burst (the coal burst discussed in this study is the strain coal burst) dynamic disasters, as shown in Figure 9(b).

From the analysis, it can be concluded that reducing the advancing velocity of the working face is likely to cause large-scale spalling of the coal wall and exposed roof, increasing the possibility of roof-fall accidents, and is not conducive to the control of the roof in the working face. Increasing the advancing velocity of the working face can reduce the failure range of the coal wall, which is beneficial for roof control, but may cause the coal to store a large amount of elastic strain energy, increasing the possibility of a coal burst at the working face. Thus, in deep coal mining, the advancing velocity of the working face can be appropriately accelerated to facilitate roof control of the working face; however, timely monitoring and appropriate measures should be taken to prevent coal burst disasters.

5. Conclusions

(1) As the loading rate increases, the peak strength of the sample generally increases, but the elastic modulus of the sample does not change regularly. Increasing the loading rate rapidly produces a large amount of damage inside the sample, accelerating the transformation of internal damage to macroscopic failure. The loading rate exhibits no obvious effect on the ratio of the damage threshold to the corresponding peak strength; the ratio is between 0.6 and 0.7.

(2) At low loading rates, cracks easily penetrate the upper and lower ends of the sample, and the failure range is wide. The sample primarily exhibits static failure, and the failure form is spalling. At high loading rates, cracks coalesce locally in the sample, and the failure range is narrow. The sample primarily exhibits dynamic failure, and the failure form is ejection of slabs and debris. A greater loading rate results in a more violent ejection failure, and thinner slabs are produced.

(3) For the deep stope, reducing the advancing velocity of the working face causes large-scale coal wall spalling, which can cause the roof at the front of the support to be exposed and induce roof fall. Increasing the advancing velocity of the working face can reduce the failure range of the coal and help prevent a roof fall, but may increase the risk of a coal burst.

Data Availability

The data used to support the findings of this study are included within the article.

Conflicts of Interest

The authors declare that they have no conflicts of interest.

Acknowledgments

References

[1] H. Xie, M. Gao, R. Zhang, G. Peng, W. Wang, and A. Li, "Study on the mechanical properties and mechanical response of coal mining at 1000 m or deeper," *Rock Mechanics and Rock Engineering*, vol. 52, no. 5, pp. 1475–1490, 2019.

[2] E. Unal, I. Ozkan, and G. Cakmakci, "Modeling the behavior of longwall coal mine gate roadways subjected to dynamic loading," *International Journal of Rock Mechanics and Mining Sciences*, vol. 38, no. 2, pp. 181–197, 2001.

[3] X. S. Liu, D. Y. Fan, Y. L. Tan et al., "Failure evolution and instability mechanism of surrounding rock for close-distance chambers with super-large section in deep coal mines," *International Journal of Geomechanics*, vol. 21, no. 5, Article ID 04021049, 2021.

[4] F. Du, K. Wang, G. Wang, Y. Huang, and L. Yi, "The mechanism of damage in gas-bearing coal-rock combination bodies and gas seepage in coals," *Energy Sources, Part A: Recovery, Utilization, and Environmental Effects*, vol. 43, no. 10, pp. 1181–1201, 2021.

[5] H. Wu, D. Ma, and G. Y. Zhao, "Fracture response and mechanisms of brittle rock with different numbers of openings under uniaxial loading," *Geomechanics and Engineering*, vol. 25, no. 6, pp. 481–493, 2021.

[6] D. Ma, H. Duan, J. Liu, X. Li, and Z. Zhou, "The role of gangue on the mitigation of mining-induced hazards and environmental pollution: an experimental investigation," *The Science of the Total Environment*, vol. 664, no. 10, pp. 436–448, 2019.

[7] Y. Luo, F.-q. Gong, X.-b. Li, and S. Wang, "Experimental simulation investigation of influence of depth on spalling characteristics in circular hard rock tunnel," *Journal of Central South University*, vol. 27, no. 3, pp. 891–910, 2020.

[8] Y. Luo, "Influence of water on mechanical behavior of surrounding rock in hard-rock tunnels: an experimental simulation," *Engineering Geology*, vol. 277, Article ID 105816, 2020.

[9] X. Si, L. Huang, X. Li, C. Ma, and F. Gong, "Experimental investigation of spalling failure of D-shaped tunnel under three-dimensional high-stress conditions in hard rock," *Rock Mechanics and Rock Engineering*, vol. 54, no. 6, pp. 3017–3038, 2021.

[10] C. Wang, A. Cao, C. Zhang, and I. Canbulat, "A new method to assess coal burst risks using dynamic and static loading analysis," *Rock Mechanics and Rock Engineering*, vol. 53, no. 3, pp. 1113–1128, 2020.

[11] Y. Jiang, H. Wang, S. Xue, Y. Zhao, J. Zhu, and X. Pang, "Assessment and mitigation of coal bump risk during extraction of an island longwall panel," *International Journal of Coal Geology*, vol. 95, pp. 20–33, 2012.

[12] F. Gong, Y. Wang, Z. Wang, J. Pan, and S. Luo, "A new criterion of coal burst proneness based on the residual elastic energy index," *International Journal of Mining Science and Technology*, vol. 31, no. 4, pp. 553–563, 2021.

[13] X. F. Si and F. Q. Gong, "Strength-weakening effect and shear-tension failure mode transformation mechanism of rockburst for fine-grained granite under triaxial unloading compression," *International Journal of Rock Mechanics and Mining Sciences*, vol. 131, Article ID 104347, 2020.

[14] D. Ma, S. Kong, Z. Li, Q. Zhang, Z. Wang, and Z. Zhou, "Effect of wetting-drying cycle on hydraulic and mechanical properties of cemented paste backfill of the recycled solid wastes," *Chemosphere*, vol. 282, Article ID 131163, 2021.

[15] F. Q. Gong, H. Ye, and Y. Luo, "The effect of high loading rate on the behaviour and mechanical properties of coal-rock combined body," *Shock and Vibration*, vol. 27, no. 3, pp. 891–910, 2020.

[16] X. Liu, S. Song, Y. Tan et al., "Similar simulation study on the deformation and failure of surrounding rock of a large section chamber group under dynamic loading," *International Journal of Mining Science and Technology*, vol. 31, no. 3, pp. 495–505, 2021.

[17] C. Xin, K. Wang, F. Du, X. Zhang, G. Wang, and Y. Liu, "Mechanical properties and permeability evolution of gas-bearing coal under phased variable speed loading and unloading," *Arabian Journal of Geosciences*, vol. 11, no. 23, p. 747, 2018.

[18] S. Wang, D. Elsworth, and J. Liu, "Mechanical behavior of methane infiltrated coal: the roles of gas desorption, stress level and loading rate," *Rock Mechanics and Rock Engineering*, vol. 46, no. 5, pp. 945–958, 2013.

[19] D. Ma, J. X. Zhang, H. Y. Duan et al., "Reutilization of gangue wastes in underground backfilling mining: overburden aquifer protection," *Chemosphere*, vol. 264, Article ID 128400, 2021.

[20] B. Huang and J. Liu, "The effect of loading rate on the behavior of samples composed of coal and rock," *International Journal of Rock Mechanics and Mining Sciences*, vol. 61, pp. 23–30, 2013.

[21] S. Okubo, K. Fukui, and Q. Qingxin, "Uniaxial compression and tension tests of anthracite and loading rate dependence of peak strength," *International Journal of Coal Geology*, vol. 68, no. 3-4, pp. 196–204, 2006.

[22] P. Huang, J. Zhang, N. J. Damascene, Z. Wang, and M. Li, "Effect of loading rate on mechanical behavior of coal samples with initial damage accumulation," *Mechanics of Time-dependent Materials*, 2021.

[23] H. M. Li, H. G. Li, B. B. Gao, D. J. Jiang, and J. F. Feng, "Study of acoustic emission and mechanical characteristics of coal samples under different loading rates," *Shock and Vibration*, vol. 2015, Article ID 458519, 11 pages, 2015.

[24] T. Ai, R. Zhang, J. F. Liu, and L. Ren, "Space-time evolution rules of acoustic emission location of unloaded coal sample at different loading rates," *International Journal of Mining Science and Technology*, vol. 22, pp. 847–854, 2012.

[25] T. Chen, Q. Yao, F. Wei et al., "Effects of water intrusion and loading rate on mechanical properties of and crack propagation in coal-rock combinations," *Journal of Central South University*, vol. 24, no. 2, pp. 423–431, 2017.

[26] N. Wang, Y. Q. Xu, D. Y. Zhu, N. Wang, and B. F. Yu, "Acoustic emission and failure modes for coal-rock structure under different loading rates," *Advances in Civil Engineering*, vol. 2018, Article ID 9391780, 11 pages, 2018.

[27] G. W. Li, S. F. Lu, S. F. Liu, J. Liu, P. Shi, and B. W. Fan, "Application and effect of loading rates on coal sample failure," *Shock and Vibration*, vol. 2021, Article ID 6681082, 12 pages, 2021.

[28] W. Xiao, D. Zhang, Y. Cai, and Y. Chu, "Study on loading rate dependence of the coal failure process based on uniaxial compression test," *Pure and Applied Geophysics*, vol. 177, no. 10, pp. 4925–4941, 2020.

[29] J. Lu, D. M. Zhang, G. Huang, X. Li, H. Gao, and G. Z. Yin, "Effects of loading rate on the compound dynamic disaster in deep underground coal mine under true triaxial stress," *International Journal of Rock Mechanics and Mining Sciences*, vol. 134, Article ID 104453, 2020.

[30] Y. Zhao, G.-F. Zhao, and Y. Jiang, "Experimental and numerical modelling investigation on fracturing in coal under impact loads," *International Journal of Fracture*, vol. 183, no. 1, pp. 63–80, 2013.

[31] M. Alber, R. Fritschen, M. Bischoff, and T. Meier, "Rock mechanical investigations of seismic events in a deep longwall coal mine," *International Journal of Rock Mechanics and Mining Sciences*, vol. 46, no. 2, pp. 408–420, 2009.

[32] H. T. Li, H. W. Zhou, Y. D. Jiang, and H. W. Wang, "An evaluation method for the bursting characteristics of coal under the effect of loading rate," *Rock Mechanics and Rock Engineering*, vol. 49, pp. 3281–3291, 2016.

[33] S.-Q. Yang, P. Xu, and T. Xu, "Nonlinear visco-elastic and accelerating creep model for coal under conventional triaxial compression," *Geomechanics and Geophysics for Geo-Energy and Geo-Resources*, vol. 1, no. 3-4, pp. 109–120, 2015.